nature biotechnology

Article

https://doi.org/10.1038/s41587-025-02556-5

Safer non-viral DNA delivery using lipid nanoparticles loaded with endogenous anti-inflammatory lipids

Received: 2 June 2024

Accepted: 8 January 2025

Published online: 05 February 2025

Check for updates

Manthan N. Patel[1,2,5], Sachchidanand Tiwari[2,3,5], Yufei Wang[2], Sarah O'Neill[1,2], Jichuan Wu[2], Serena Omo-Lamai[2,4], Carolann Espy[1,2], Liam S. Chase[2,4], Aparajeeta Majumder[2], Evan Hoffman[2], Anit Shah[2], András Sárközy[3], Jeremy Katzen[2], Norbert Pardi[3] & Jacob S. Brenner[1,2]

The value of lipid nanoparticles (LNPs) for delivery of messenger RNA (mRNA) was demonstrated by the coronavirus disease 2019 (COVID-19) mRNA vaccines, but the ability to use LNPs to deliver plasmid DNA (pDNA) would provide additional advantages, such as longer-term expression and availability of promoter sequences. However, pDNA-LNPs face substantial challenges, such as toxicity and low delivery efficiency. Here we show that pDNA-LNPs induce acute inflammation in naive mice that is primarily driven by the cGAS–STING pathway. Inspired by DNA viruses that inhibit this pathway for replication, we loaded endogenous lipids that inhibit STING into pDNA-LNPs. Loading nitro-oleic acid (NOA) into pDNA-LNPs (NOA-pDNA-LNPs) ameliorated serious inflammatory responses in vivo, enabling safer, prolonged transgene expression—11.5 times greater than that of mRNA-LNPs at day 32. Additionally, we performed a small LNP formulation screen to iteratively optimize transgene expression and increase expression 50-fold in vitro. pDNA-LNPs loaded with NOA and other bioactive molecules should advance genetic medicine by enabling longer-term and promoter-controlled transgene expression.

The success of the coronavirus disease 2019 (COVID-19) vaccines showed the unprecedented power of lipid nanoparticles (LNPs) to deliver nucleic acids to target cells, driving expression of encoded proteins higher than with prior non-viral technologies[1]. The ability to target LNPs to specific organs and cell types is enabling applications in many diseases[2]. In the COVID-19 vaccines and many other applications of LNPs, the nucleic acid cargo has been messenger RNA (mRNA) or small interfering RNA (siRNA), which can transiently express encoded proteins or knock down endogenous proteins, respectively. However, mRNA has a relatively short half-life (~hours), lacks a promoter region to achieve cell-type-specific and temporal control and is not stable for long at room temperature or 4 °C (ref. 3). DNA could overcome many of the challenges associated with the use of mRNA and, thereby, open up more applications for LNPs. DNA can express transgene proteins for several months[4], has a promoter that can be made cell type specific and/or turned on/off with small-molecule drugs (such as a doxycycline-sensitive promoter)[5] and can be stored for months at 4 °C. Such advantages could broaden LNP applications to include long-term expression of therapeutic proteins

[1]Department of Systems Pharmacology and Translational Therapeutics, Perelman School of Medicine, University of Pennsylvania, Philadelphia, PA, USA. [2]Division of Pulmonary, Allergy, and Critical Care, Department of Medicine, Perelman School of Medicine, University of Pennsylvania Philadelphia, Philadelphia, PA, USA. [3]Department of Microbiology, Perelman School of Medicine, University of Pennsylvania, Philadelphia, PA, USA. [4]Department of Bioengineering, School of Engineering & Applied Science, University of Pennsylvania, Philadelphia, PA, USA. [5]These authors contributed equally: Manthan N. Patel, Sachchidanand Tiwari. e-mail: jacob.brenner@pennmedicine.upenn.edu

https://doi.org/10.1038/s41587-025-02556-5

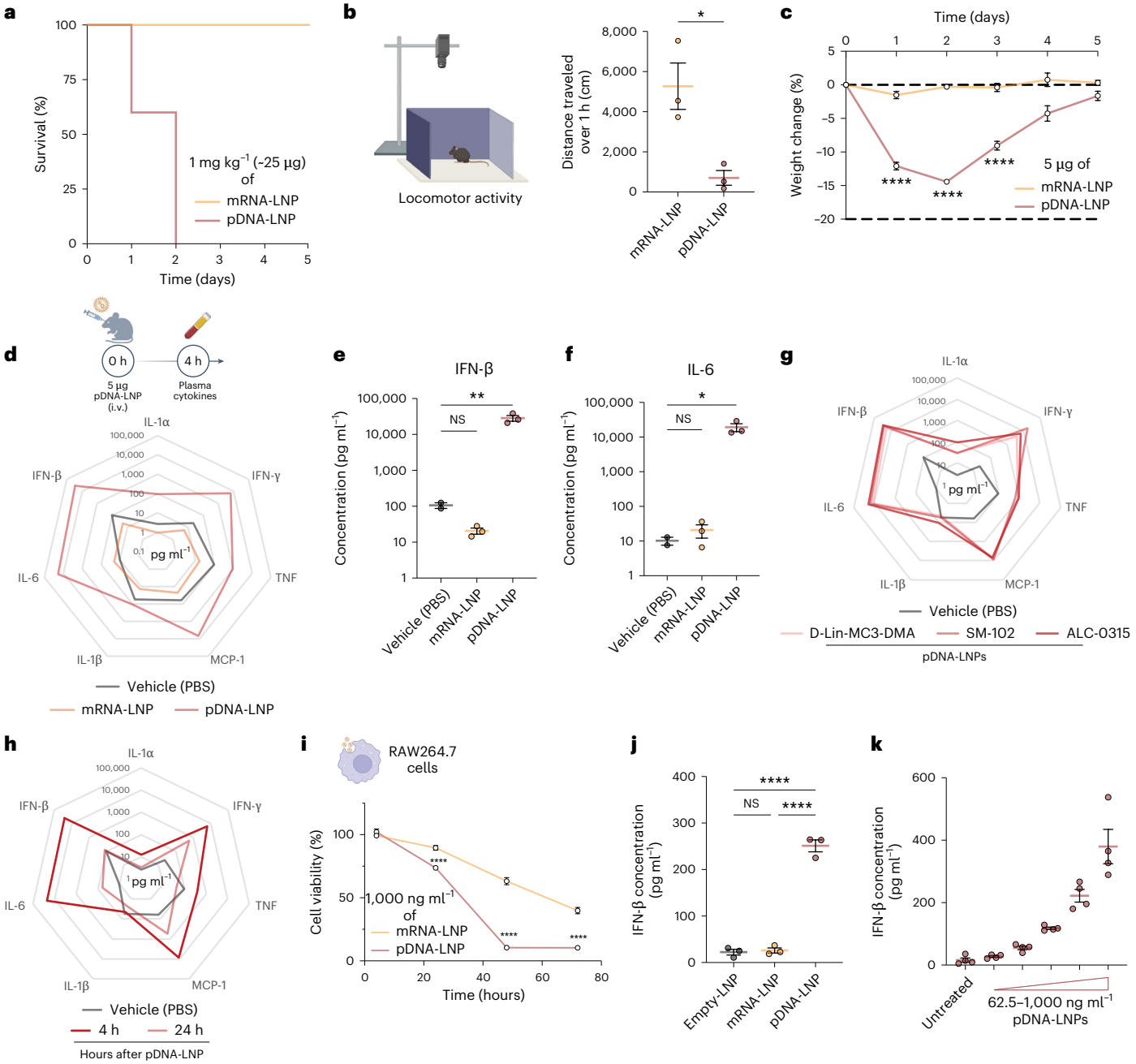

Fig. 1 | Unlike nucleoside-modified mRNA-LNP, pDNA-LNP delivery causes acute inflammatory responses. a, Survival curve graph of naive C57BL/6 ('Black-6') mice i.v. injected with 1 mg kg^{-1} of either mRNA-LNP or pDNA-LNP shows 100% mortality in mice treated with pDNA-LNPs compared with 0% in mice treated with mRNA-LNPs. **b**, Four hours after 1 mg kg^{-1} i.v. injection of LNPs, movement of mice was tracked for 1 h, and total distance walked was assessed by AI software (DeepLabCuts), a validated metric of an infusion reaction. Mice treated with pDNA-LNPs had significantly lower total distance walked compared with mRNA-LNP controls, indicating severe lethargy. **c**, Weight change over time in mice given a much lower i.v. dose (5 µg) of mRNA-LNPs or pDNA-LNPs. **d**, Multiplex analysis of pro-inflammatory plasma cytokines 4 h after a 5 µg i.v. dose of pDNA-LNP indicates acute systemic inflammation compared with PBS and mRNA-LNP controls. **e**,**f**, Specifically, IFN-β (**e**) and IL-6 (**f**) levels were approximately 1,400-fold and approximately 1,000-fold higher, respectively, for mice injected with pDNA-LNP compared with mRNA-LNP. **g**, Five micrograms of pDNA formulated with three FDA-approved LNP formulations (D-Lin-MC3-DMA, SM-102 and ALC-0315 ionizable lipids) was i.v. injected in mice, and plasma was collected 4 h later for cytokine quantification, which indicated that this inflammatory response occurs across various LNP formulations. **h**, Cytokine levels in mouse plasma collected 4 h or 24 h after i.v. injection of 5 µg of pDNA-LNPs, highlighting acute-but-transient inflammation, with the majority of pro-inflammatory cytokine levels back to baseline at the 24 h timepoint. **i**–**k**, In vitro studies in a macrophage-derived cell line, RAW264.7. **i**, Effect of 1,000 ng ml^{-1} mRNA-LNP or pDNA-LNP on cell viability over time. **j**, IFN-β levels in cell supernatant 4 h after exposure to 1,000 ng ml^{-1} of empty-LNP, mRNA-LNP and pDNA-LNP show DNA-cargo-specific inflammatory cytokine production. **k**, IFN-β levels in cell supernatant increase exponentially as a function of pDNA-LNP dose. Statistics: $n = 5$ per group for **a** and **c** (biological replicates); $n = 4$ per group for **k** (biological replicates); and $n = 3$ per group for the rest (biological replicates). Data shown represent mean ± s.e.m. **b**,**c**,**i**, Unpaired, two-tailed t-tests were performed. For all other graphs, comparisons were made using one-way ANOVA with Tukey's post hoc test. *$P < 0.05$, **$P < 0.01$ and ****$P < 0.0001$. NS, not significant.

such as monoclonal antibodies, secreted proteins or even intracellular proteins, reducing concerns about the half-life of the engineered proteins because of constant protein production. Additionally, DNA can be used to express short-hairpin RNA (shRNA; to knock down proteins long term), gene editing proteins and guide RNAs.

For each of these genetic cargos, DNA-loaded LNPs (DNA-LNPs) would offer the advantages of long-term expression (and, thus, infrequent dosing) along with the advantages that LNPs already provide, including high levels of expression, low immunogenicity (compared with viral vectors)[6] and fewer limitations on cargo size[7]. These benefits could enable treatment of diseases that are less accessible to mRNA-LNPs, such as diseases of chronic autoimmunity, degeneration, pain and more. Since the clinical development of LNPs in the past decade, there have been very few reports on DNA delivery, primarily focusing on vaccine applications or LNP formulation screening[8–11].

Here we begin by showing that this lack of study is likely because plasmid DNA delivered via LNPs (pDNA-LNPs) is highly inflammatory and induces mortality at commonly used therapeutic doses in naive mice. Through in vitro immunostaining and an in vivo knockout mouse model, we found that this inflammation is largely driven by activation of the cyclic GMP-AMP synthase (cGAS) and stimulator of interferon genes (STING) signaling pathway. cGAS is a cytosolic DNA sensor that recognizes DNA via electrostatic interactions[12]. Upon DNA binding, cGAS activates downstream STING signaling, which leads to inflammation characterized by upregulation of type 1 interferons (IFNs), such as IFN-β, and pro-inflammatory cytokines, such as interleukin 6 (IL-6)[13]. As cGAS can detect DNA in a sequence-independent manner, we pursued an alternative strategy to mitigate pDNA-induced inflammation: loading naturally occurring STING inhibitors into pDNA-LNPs to enable safe and effective delivery.

We loaded nitro-oleic acid (NOA), an endogenous anti-inflammatory lipid that inhibits STING[14], into pDNA-LNPs (NOA-pDNA-LNPs). This led to undetectable levels of pDNA-induced STING activation in vitro. Whereas standard pDNA-LNPs injected intravenously (i.v.) at 1 mg kg^{-1} dose into naive C57BL/6 mice induced 100% mortality (physiological death) within 2 d, NOA-pDNA-LNPs induced 0% mortality. We then showed that the addition of NOA in pDNA-LNPs does not hinder transgene expression and enables prolonged protein expression (at least 1 month). Additionally, we showed the potential to further optimize the nascent technology of pDNA-LNPs, as a small LNP formulation screen improved the transgene expression capacity of NOA-pDNA-LNPs 50-fold in vitro, enabling NOA-pDNA-LNPs to achieve similar transfection efficiencies to one of the gold standard in vitro transfection reagents, Lipofectamine, in a cell type that is widely considered difficult to transfect: human induced pluripotent stem cell (iPSC)-derived type II alveolar epithelial cells (iAT2s). Overall, these results show that NOA-pDNA-LNPs, and, more generally, pDNA-LNPs loaded with bioactive molecules, have the potential to provide safe, long-term expression of therapeutic cargo.

Results

Unlike nucleoside-modified mRNA-LNPs, pDNA-LNPs induce acute inflammatory responses

To systematically probe inflammation, we used BioNTech/Pfizer's FDA-approved COVID-19 mRNA vaccine LNP formulation, containing the ionizable lipid ALC-0315, formulated with either 5moU nucleoside-modified mRNA or pDNA. To minimize carrier side effects as a confounding variable, both mRNA-LNPs and pDNA-LNPs were formulated using 40-to-1 total lipid-to-nucleic acid ratio (w/w, or N:P of 9.7).

After i.v. injecting a commonly used therapeutic dose[15] of 1 mg kg^{-1} (~25 µg pDNA per mouse) into naive C57BL/6 mice, we observed 100% mortality (physiological death) within 2 d for mice that received pDNA-LNPs compared with 0% for mice that received mRNA-LNPs (Fig. 1a). Furthermore, we noticed extreme lethargy and lack of movement of mice 4 h after pDNA-LNP administration, using an artificial intelligence (AI) motion-tracking device that we previously validated for detecting infusion reactions[16] (Fig. 1b). Thus, LNPs delivering pDNA at a 1 mg kg^{-1} dose, but not nucleoside-modified mRNA at the same dose, induce an acute inflammatory reaction that leads to physiological death within 2 d in naive mice. We also found that 1 mg kg^{-1} pDNA-LNPs also induce a high mortality rate when administered intramuscularly (i.m.) compared with mRNA-LNP control (Supplementary Fig. 1a). Furthermore, we administered mRNA-LNPs and pDNA-LNPs intratracheally (i.t.) and evaluated inflammation specific to the lungs by examining protein and leukocyte levels in the bronchoalveolar lavage (BAL) fluid, which indicates capillary leakage and leukocyte penetration into the alveoli (air sacs). We observed higher levels of protein, total cells and pro-inflammatory cytokines in the BAL from mice that received pDNA-LNPs compared with mRNA-LNPs, highlighting pDNA's cargo-induced inflammatory responses (Supplementary Fig. 1b–d).

To study the mechanisms underlying pDNA-LNP-induced inflammation, we reduced the pDNA-LNP dose five-fold to 5 µg of pDNA per mouse, ensuring survival and enabling assessment of signaling pathways. Just 1 d after the administration of 5 µg of pDNA-LNP, the mice lost more than 10% of their body weight, taking approximately 5 d to return to baseline levels (Fig. 1c). Furthermore, to assess systemic inflammation, we collected plasma 4 h after the pDNA-LNP i.v. injection and observed a significant increase in the levels of various pro-inflammatory cytokines (Fig. 1d). Specifically, IFN-β and IL-6 plasma concentrations increased 1,400-fold and 1,000-fold, respectively, compared with the mRNA-LNP-treated group (Fig. 1e,f). Thus, LNPs loaded with pDNA, but not with nucleoside-modified mRNA, induced a massive cytokine response. Notably, IFN-β is a type 1 IFN that is traditionally known as an antiviral cytokine[17], hinting that the immune system likely identifies pDNA-LNP administration as a viral infection. To ensure that pDNA-LNP toxicity was independent of LNP formulation, we synthesized pDNA-LNPs using two other FDA-approved LNP formulations (D-Lin-MC3-DMA and SM-102 ionizable lipids)[18,19]. Regardless of LNP formulation, we observed acute inflammation in vivo (Fig. 1g). Moreover, we observed similar inflammatory responses in LNPs loaded with various plasmids (Supplementary Fig. 2) and in both male and female mice (Supplementary Fig. 3).

We next investigated the kinetics of the inflammatory response as the mice returned to a normal visual and behavioral phenotype 24 h after pDNA-LNP administration. In agreement with our visual assessment, we observed a decrease in most pro-inflammatory cytokines in the plasma 24 h after the 5 µg pDNA-LNP dose, with the majority of cytokines, specifically, IFN-β and IL-6, back to baseline levels (Fig. 1h). Furthermore, we ensured that inflammation does not reappear at later

Fig. 2 | STING activation drives pDNA-LNP-induced inflammation. a, The proposed mechanism that drives pDNA-LNP inflammation. Any cytosolic DNA (endogenous or exogenous) is detected, independent of DNA sequence, by cGAS, leading to downstream activation of STING, which induces an acute inflammatory response. **b**, STING-KO mice i.v. injected with 5 µg of pDNA-LNPs have reduced levels of pro-inflammatory cytokines in plasma 4 h after dose compared with wild-type mice. **c**,**d**, pDNA-LNPs injected in STING-KO mice have complete reduction in IFN-β (**c**), leading to improved survival rates at the 1 mg kg^{-1} dose (**d**). **e**, Representative images of p-STING 4 h after treatment indicate STING activation for the pDNA group (1,000 ng ml^{-1} dose) in RAW264.7 cells. **f**, Quantification of p-STING MFI from original images. Statistics: $n = 3$ per group for **b** and **c** (biological replicates); $n = 5$ per group for **d** (biological replicates); and $n = 6$ per group for **f** (biological replicates). Data shown represent mean ± s.e.m. **c**, Unpaired, two-tailed t-test was performed. **f**, Comparisons were made using one-way ANOVA with Tukey's post hoc test. All studies were done using C57BL/6 mice. *$P < 0.05$, **$P < 0.01$ and ***$P < 0.001$.

https://doi.org/10.1038/s41587-025-02556-5

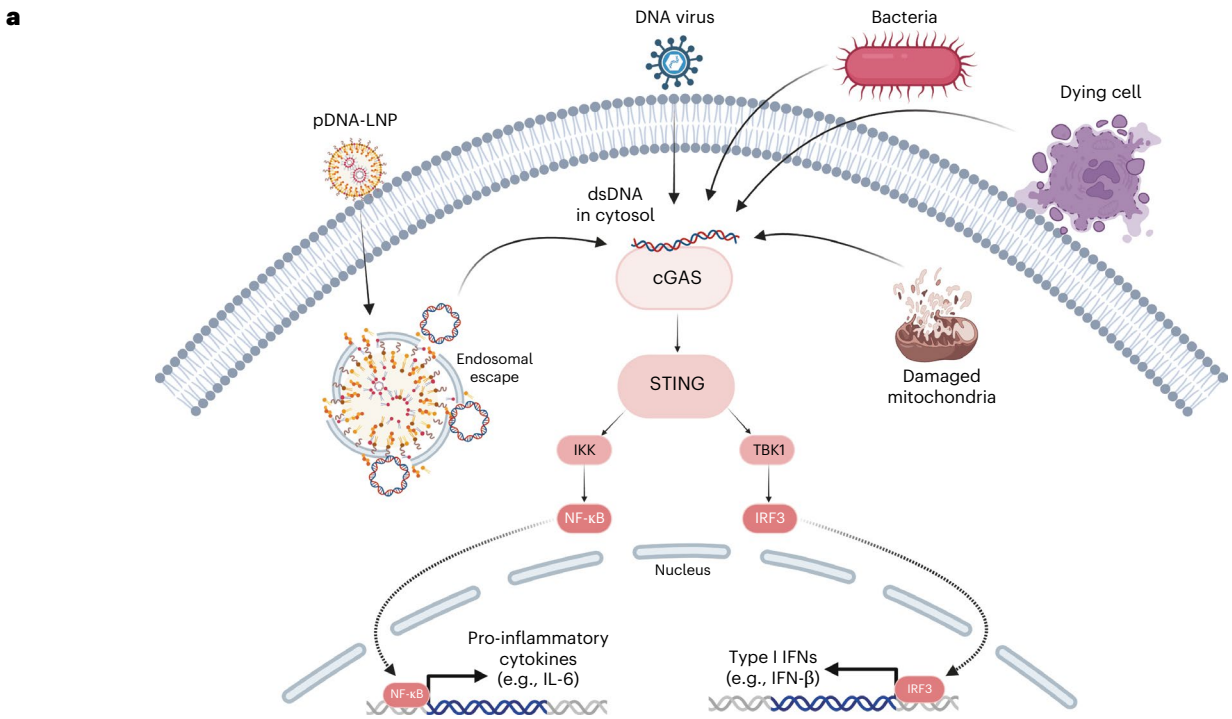

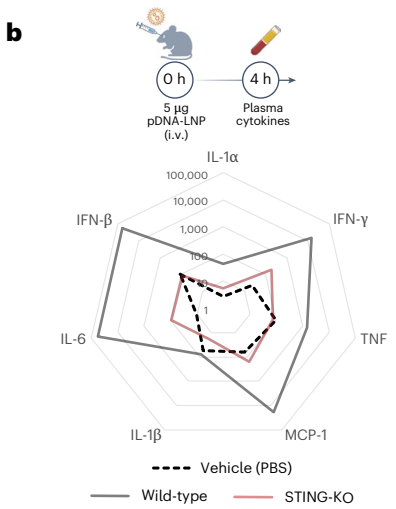

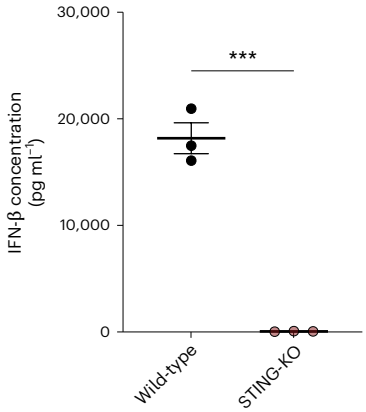

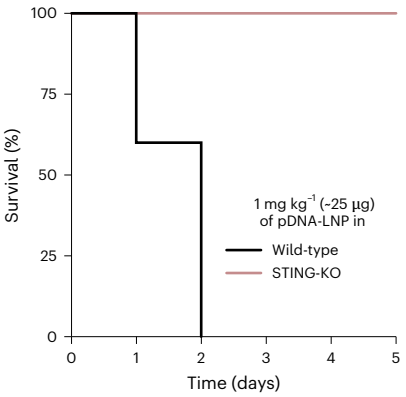

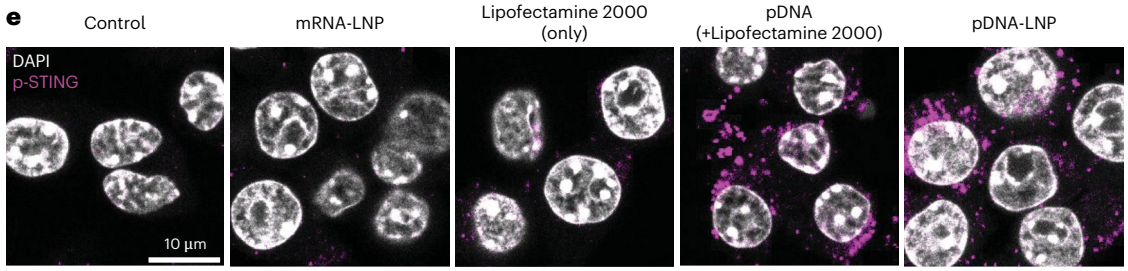

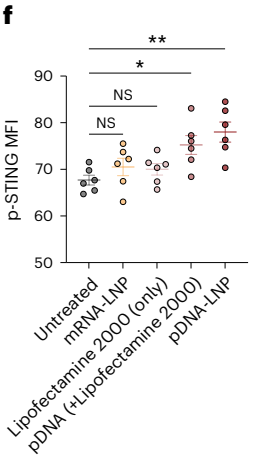

https://doi.org/10.1038/s41587-025-02556-5

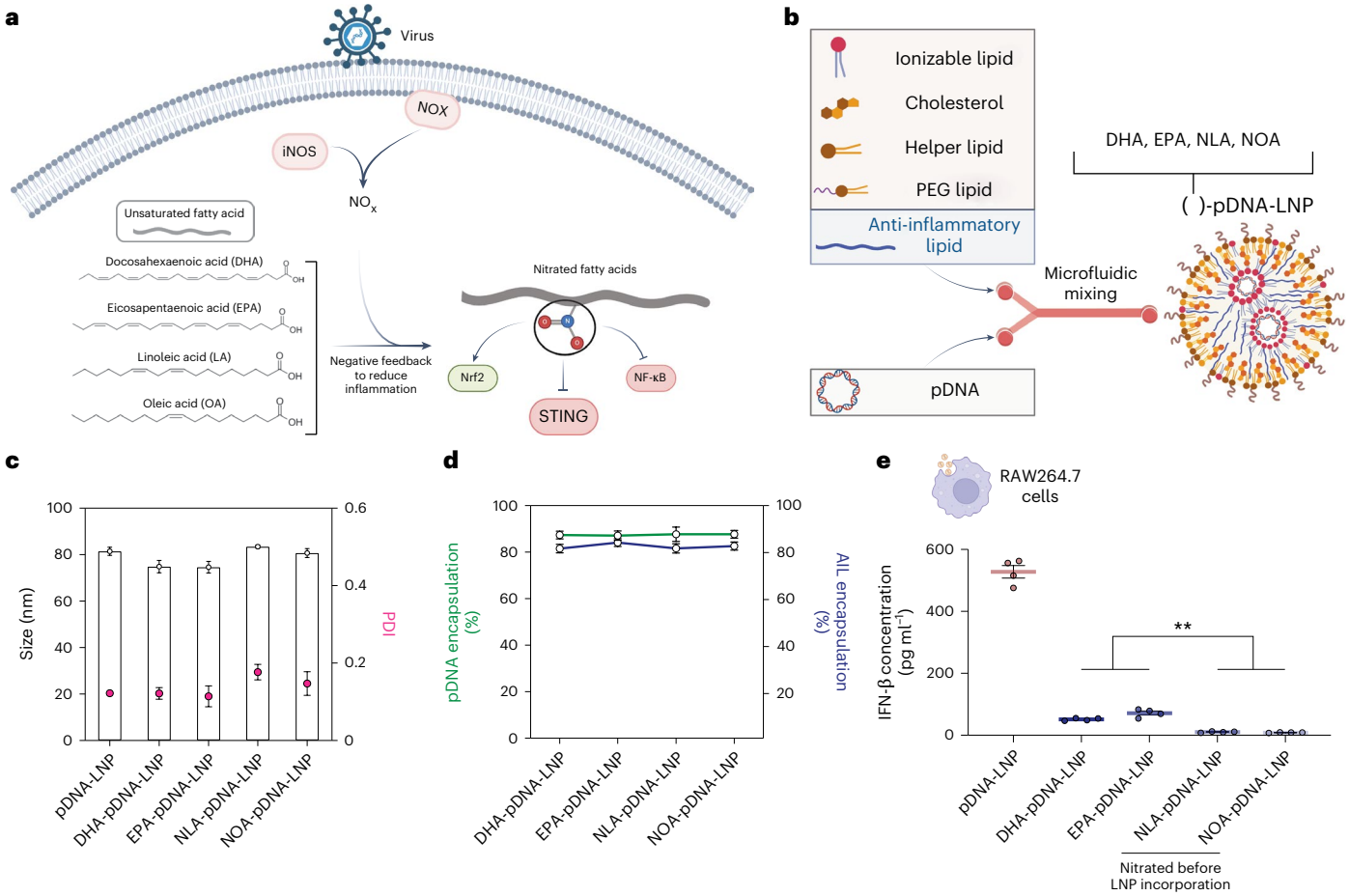

Fig. 3 | Loading endogenous anti-inflammatory lipids that inhibit STING into standard pDNA-LNP formulations. a, Schematic showing how cell stress caused by virus infections leads to nitration of endogenous unsaturated fatty acids to form NFAs that have anti-inflammatory properties, including potent inhibition of STING (modified from Fig. 1 of the article by Hansen et al.[14]). **b**, Development of platform technology by adding AILs as the fifth component in the lipid mixture before LNP formation using microfluidics. **c**, Size distribution of pDNA-LNPs loaded with various AILs determined by DLS shows no differences in LNP size or polydispersity index (PDI). **d**, All tested AILs load more than 80% (AIL-to-lipid ratio of 0.2, mole-to-mole) and have no impact on pDNA encapsulation. Detailed methodology can be found in Methods. **e**, pDNA-LNPs loaded with various AILs reduce IFN-β levels in cell supernatant 4 h after 1,000 ng ml^{-1} dose. AILs that are nitrated before LNP formation (NLA and NOA) are more effective than lipids that are not nitrated during LNP formation (DHA and EPA). Statistics: $n = 4$ per group for **e** (biological replicates) and $n = 3$ per group for **c** and **d** (technical replicates, similar findings with biological replicates). Data shown represent mean ± s.e.m., and comparisons were made using one-way ANOVA with Tukey's post hoc test. $^{**}P < 0.01$.

timepoints by measuring plasma cytokines 5 d after pDNA-LNP administration (Supplementary Fig. 4). Because this response was acute, we investigated if pDNA-LNPs are inflammatory in innate immune cells such as macrophages that we previously showed are key in mediating acute LNP carrier-related toxicities and are known to sensitively detect DNA viruses[20,21].

We treated the macrophage-derived cell line RAW264.7 with various concentrations of pDNA-LNPs, for various treatment times, and measured cell viability (Supplementary Fig. 5). At a concentration of 1,000 ng ml^{-1} for both mRNA-LNPs and pDNA-LNPs, we found a significant decrease in cell viability over time, with approximately 90% cell death 48 h after pDNA-LNP compared with less than 50% after mRNA-LNP treatment (Fig. 1i). Moreover, similarly to the in vivo cytokine results, we observed a significant increase (~10-fold) in IFN-β levels in the cell supernatant for pDNA-LNPs compared with empty-LNP and mRNA-LNP controls 4 h after 1,000 ng ml^{-1} LNP treatment (Fig. 1j). Next, we performed a dose–response study of pDNA-LNPs, which showed exponential increase in IFN-β levels (Fig. 1k). Lastly, we tested non-circular DNA by linearizing pDNA (LinDNA) to have a direct comparison with the circular pDNA. We observed that toxicity and transfection efficiency in cells that received LinDNA-LNP were lower than that of cells treated with pDNA-LNP but still greater than empty-LNP and mRNA-LNP controls (Supplementary Fig. 6). We speculate that the trends in both cell viability and expression are due to increased intracellular clearance of LinDNA, as it is more degradable by exonucleases compared with circular pDNA[22].

In summary, we demonstrate that DNA-LNPs trigger acute inflammatory responses across a range of conditions, including various routes of administration, multiple LNP formulations and different plasmid backbone types, in both male and female mice and with non-circular DNA constructs.

STING activation drives pDNA-LNP-induced inflammation

Among the well-characterized DNA-sensing pathways, cGAS–STING was frequently reported to induce acute inflammatory responses and significantly upregulate type 1 IFNs in response to viral infections[12,13,17]. cGAS activation can occur not only from viral DNA but also from any cytosolic DNA[23]. Thus, it serves as a versatile sensor that can also be activated by bacterial DNA, DNA from dying cells and even self-mitochondrial DNA that is released into the cytosol during cell stress, leading to downstream activation of STING (Fig. 2a). As such, we investigated if pDNA-LNPs activate this pathway.

https://doi.org/10.1038/s41587-025-02556-5

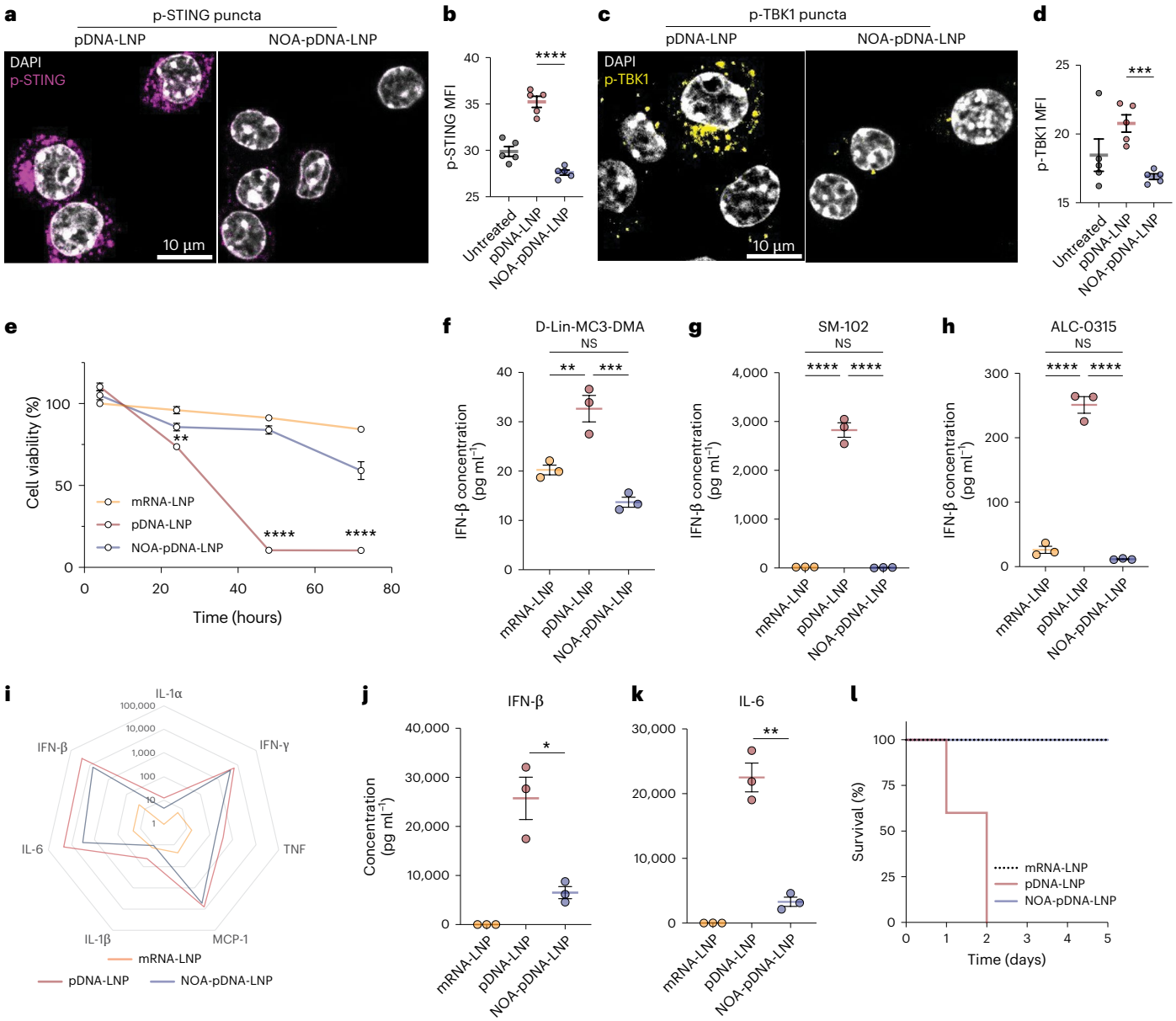

Fig. 4 | NOA-pDNA-LNPs show superior safety profiles compared with standard pDNA-LNPs in vitro and in vivo. a, Representative confocal images of p-STING show that NOA-pDNA-LNPs do not activate STING compared with standard pDNA-LNPs in RAW264.7 cells. **b**, Quantification of p-STING MFI shows significant decrease for the NOA-pDNA-LNP group relative to standard pDNA-LNP. **c**, Confocal imaging of a downstream marker of STING activation, phosphorylated TBK1 (p-TBK1), is also not activated for cells treated with NOA-pDNA-LNPs compared with standard pDNA-LNPs. **d**, Quantification of p-TBK1 MFI. **e**, RAW264.7 cell viability measured over time indicates better tolerability of NOA-pDNA-LNPs compared with standard pDNA-LNPs. **f**–**h**, IFN-β levels in cell supernatant are significantly lower for NOA-pDNA-LNPs compared with standard pDNA-LNP 4 h after 1,000 ng ml^{-1} dose, irrespective of LNP formulation (D-Lin-MC3-DMA (**f**), SM-102 (**g**) and ALC-0315 (**h**)—all FDA-approved LNP formulations). **i**, Quantification of pro-inflammatory plasma cytokines 4 h after a 5 µg dose of pDNA-LNPs or NOA-pDNA-LNPs. **j**,**k**, Specifically, IFN-β (**j**) and IL-6 (**k**) levels are approximately four-fold and approximately eight-fold lower, respectively, for mice injected i.v. with NOA-pDNA-LNP compared with standard pDNA-LNP control. **l**, Survival curve in C57BL/6 ('Black-6') mice, comparing an i.v. dose of 1 mg kg^{-1} of pDNA-LNP and NOA-pDNA-LNPs, shows that the addition of NOA in pDNA-LNPs completely prevents mortality. Statistics: $n = 5$ per group for **b** and **d** (technical replicates, similar findings with biological replicates); $n = 3$ per group for **e**–**k** (biological replicates); and $n = 5$ per group for **l** (biological replicates). Data shown represent mean ± s.e.m. **e**, Unpaired, two-tailed t-tests were performed. **b**,**d**,**f**–**h**,**j**,**k**, Comparisons were made using one-way ANOVA with Tukey's post hoc test. *$P < 0.05$, **$P < 0.01$, ***$P < 0.001$ and ****$P < 0.0001$.

To assess the role of the cGAS–STING pathway in pDNA-LNP-induced inflammation, we i.v. injected pDNA-LNPs in C57BL/6 wild-type and STING knockout (STING-KO) mice and collected plasma 4 h later. After i.v. injection of 5 µg of pDNA-LNPs, we observed significantly lower levels of various pro-inflammatory cytokines in STING-KO mice compared with wild-type mice, indicating STING activation as a primary driver of pDNA-LNP inflammation (Fig. 2b). IFN-β was at baseline levels in the STING-KO mice injected with pDNA-LNPs (Fig. 2c), leading to 100% survival rate (Fig. 2d). We also investigated two other notable DNA sensor pathways, AIM2 and TLR9 (Supplementary Fig. 7). We did not observe any significant reduction in pro-inflammatory cytokines in these two knockout mice injected with pDNA-LNPs, confirming that most pDNA-LNP-induced inflammation is largely driven by the cGAS–STING pathway.

https://doi.org/10.1038/s41587-025-02556-5

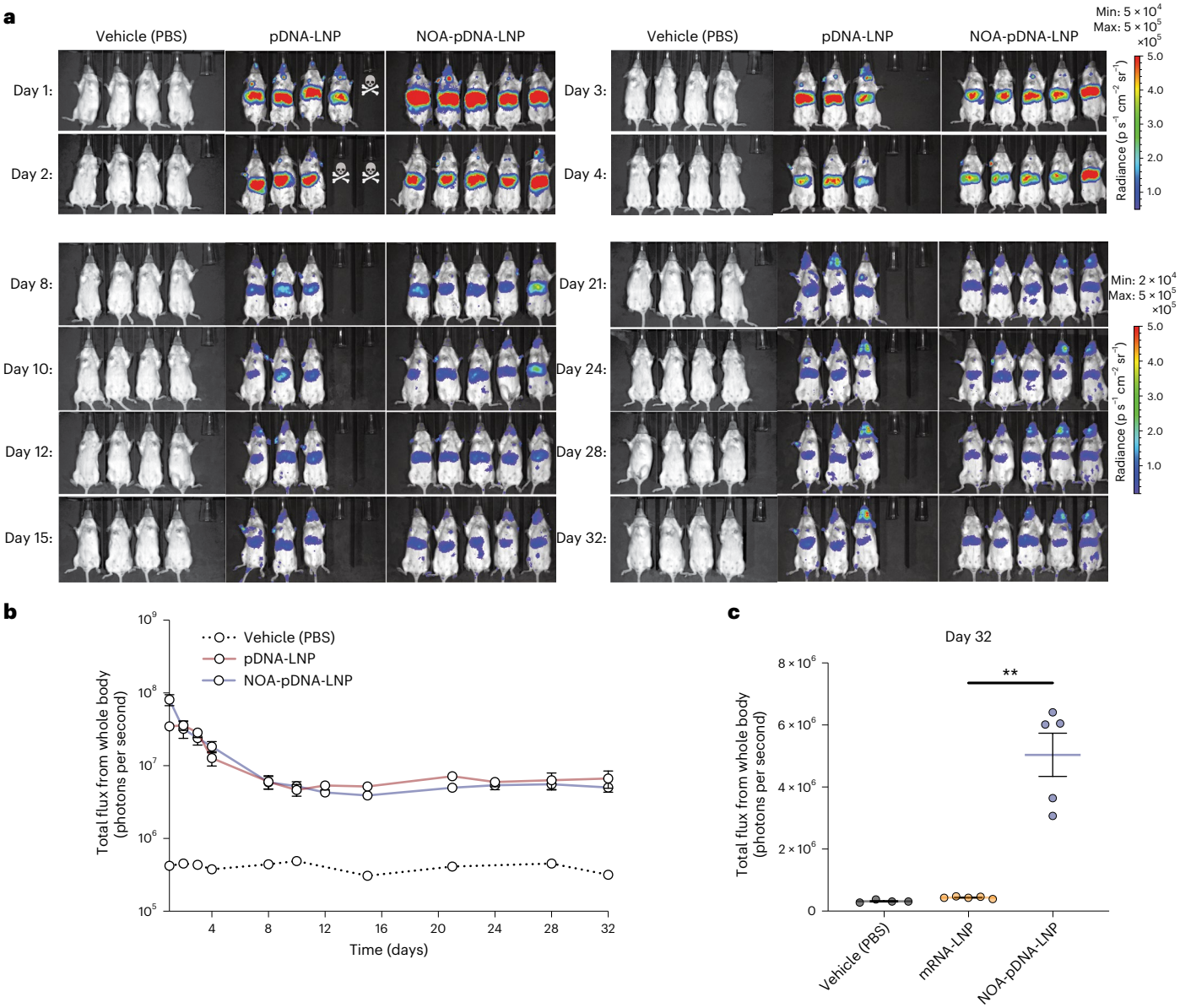

Fig. 5 | NOA-pDNA-LNPs show prolonged transgene expression in vivo. **a**, Representative IVIS images of BALB/c mice that were i.v. injected (retro-orbitally) with 25 µg of either pDNA-LNPs or NOA-pDNA-LNPs (encoding luciferase). p, photons. **b**, Quantified total flux (photons per second) from IVIS images shows that the addition of NOA does not hinder pDNA transgene expression capacity and shows prolonged expression (at least 1 month). **c**, At day 32, total transgene expression levels were significantly higher in mice treated with 25 µg NOA-pDNA-LNPs compared with PBS and mRNA-LNP (5 µg) controls. Statistics: $n = 4$ per group for PBS control group and $n = 5$ per group for pDNA-LNP and NOA-pDNA-LNP groups for **a**–**c** (biological replicates). Note that two mice that received 25 µg of pDNA-LNPs died within 2 d. Data shown represent mean ± s.e.m. **c**, Comparisons were made using one-way ANOVA with Tukey's post hoc test. $^{**}P < 0.01$.

Furthermore, we observed that the overall level of inflammation was lower in the BALB/c strain compared with the C57BL/6 strain (approximately two-fold lower IFN-β levels), although both are considerably higher than the baseline and the mRNA-LNP control (Supplementary Fig. 8a). Thus, BALB/c mice better tolerated pDNA-LNPs, as the mortality rate was 20% compared with 100% in C57BL/6 mice at the 1 mg kg^{-1} (~25 µg) dose (Supplementary Fig. 8b). Notably, BALB/c mice that survived still experienced considerable weight loss (Supplementary Fig. 8c).

In addition, using confocal microscopy, we confirmed STING activation in macrophages treated with pDNA-Lipofectamine or pDNA-LNP, by staining for activated STING (phosphorylated-STING (p-STING)) (Fig. 2e). Note that we did not see STING activation in the Lipofectamine-only and mRNA-LNP controls, indicating that it is a pDNA-specific activation rather than a carrier-based activation (Fig. 2f).

Loading of endogenous anti-inflammatory lipids that inhibit STING into standard pDNA-LNP formulations

We next looked into inhibitors of STING that we can load into standard pDNA-LNP to ameliorate its acute adverse events. We first investigated anti-inflammatory lipids (AILs) as they are highly lipophilic and have a better chance of loading into standard pDNA-LNPs compared with small-molecule drugs. We also prioritized fast-acting drugs as opposed to siRNAs, because pDNA-LNP inflammation is acute but transient, as shown previously in Fig. 1h.

Many unsaturated fatty acids, such as docosahexaenoic acid (DHA), eicosapentaenoic acid (EPA), linoleic acid (LA) and oleic acid

https://doi.org/10.1038/s41587-025-02556-5

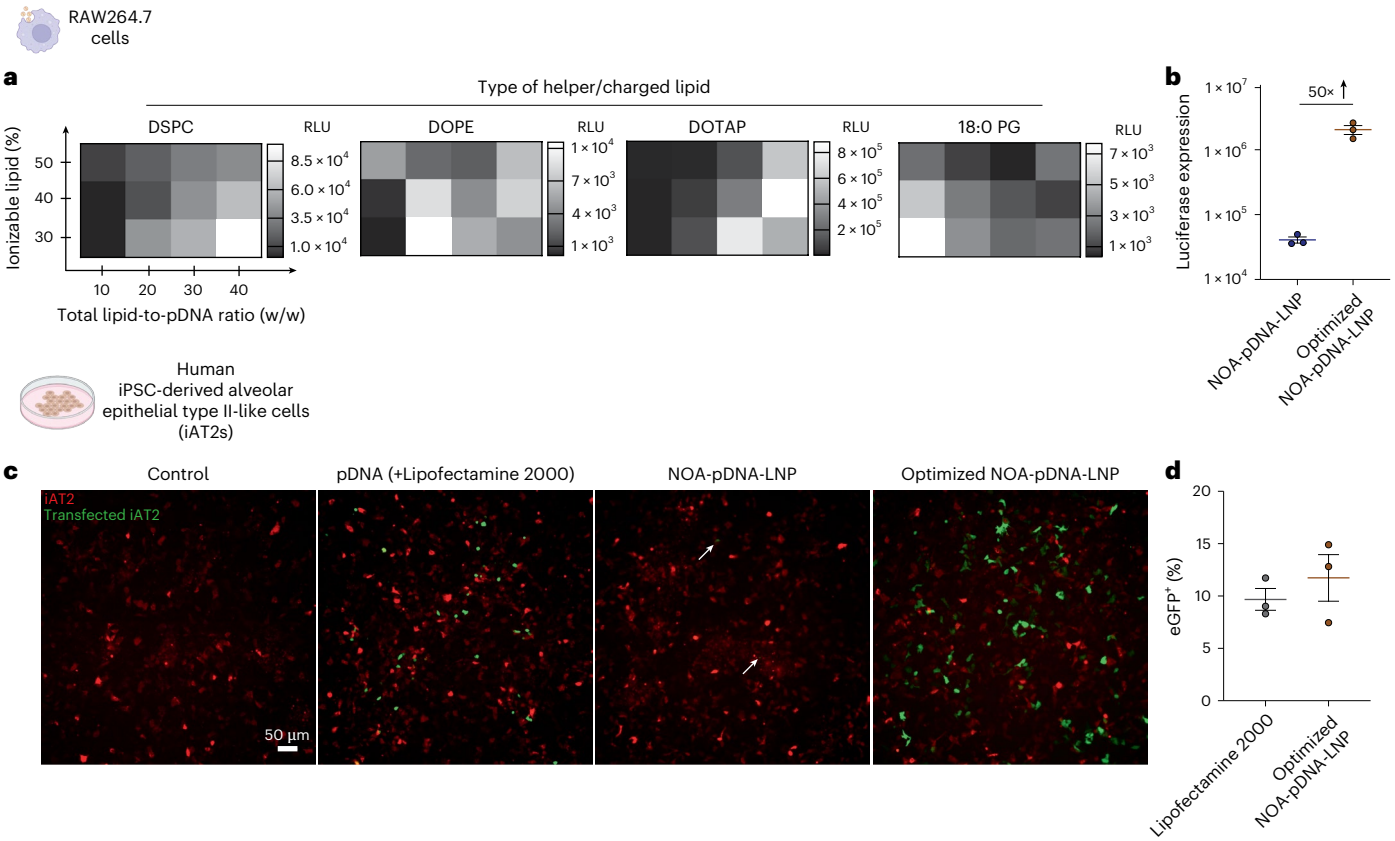

Fig. 6 | A small LNP formulation screen significantly boosts transgene expression of NOA-pDNA-LNPs in vitro, enabling efficient transfection in difficult-to-transfect cells. a,**b**, DoE screening to optimize NOA-pDNA-LNP formulation in RAW264.7 cells. Using JMP software, a full factorial screen was designed by varying ionizable lipid mol% (30–50), total lipid-to-pDNA w/w ratio (10:1 to 40:1) and the type of helper lipid used (DSPC, DOPE, DOTAP and 18:0 PG). All LNPs contained a NOA-to-total lipid ratio of 0.2 (mole-to-mole). Twenty-four hours after 500 ng ml^{-1} treatment in RAW264.7 cells, luciferase protein expression was measured, highlighting the influence of LNP formulation parameters for transgene expression (**a**). NOA-pDNA-LNP optimized with DOTAP as the helper lipid led to a 50-fold increase in transgene expression when compared with standard NOA-pDNA-LNP (**b**). **c**,**d**, Two-dimensional monoculture of difficult-to-transfect cell line human iPSC-derived type II alveolar epithelial cells (iAT2s) was treated with 1,000 ng of eGFP-encoding pDNA, using Lipofectamine, standard NOA-pDNA-LNPs or optimized NOA-pDNA-LNPs, and imaged after 48 h. tdTomato (red) signal indicates iAT2 positivity and eGFP (green) signal indicates successfully transfected cells (**c**). One hundred twenty hours after transfection, tdTomato$^+$ cells that were also eGFP$^+$ were quantified using flow cytometry, indicating similar transfection levels (trending higher) for optimized NOA-pDNA-LNPs to the gold standard, Lipofectamine 2000 (**d**). Statistics: $n = 2$ per LNP formulation for **a** (biological replicates) and $n = 3$ per group for **b**–**d** (biological replicates, representative images shown for **c**). Data shown represent mean ± s.e.m.

(OA), were found to be nitrated after a virus infection as a negative feedback loop to dampen excessive inflammation[14,24] (Fig. 3a). These nitrated fatty acids (NFAs) act as electrophiles with the ability to modify various proteins on specific exposed cysteines, leading to inhibition of nuclear factor kappa B (NF-κB), which controls an array of prototypical pro-inflammatory signaling genes, and activation of nuclear factor erythroid 2-related factor 2 (Nrf2), which controls an array of anti-oxidant response element–dependent genes[25]. Notably, NFAs are potent inhibitors of STING[14].

We loaded DHA, EPA and already nitrated versions of LA and OA (NLA and NOA, respectively) by adding these AILs as a fifth component into standard LNP formulation at an AIL-to-total lipid ratio of 0.2 (mole-to-mole) (Fig. 3b). Using dynamic light scattering (DLS), we confirmed that LNP size and polydispersity were unaffected by the addition of this fifth component (Fig. 3c). Furthermore, all AILs showed encapsulation efficiencies of more than 80% confirmed by ultra-performance liquid chromatography (UPLC) without negatively affecting pDNA loading (Fig. 3d). UPLC chromatogram of NOA is shown in Supplementary Fig. 9.

To initially assess the safety profile of AIL-loaded pDNA-LNPs, we treated RAW264.7 cells with a 1,000 ng ml^{-1} dose and quantified IFN-β levels in the cell supernatant 4 h after treatment. All AIL-loaded pDNA-LNPs had considerably reduced IFN-β levels compared with standard pDNA-LNPs (Fig. 3e). Furthermore, pDNA-LNPs loaded with NLA or NOA (lipids nitrated before LNP incorporation) performed better than pDNA-LNPs loaded with DHA or EPA. Note that we did not observe a decrease in cell viability of NOA-pDNA-LNPs 4 h after treating at 1,000 ng ml^{-1} dose (Supplementary Fig. 10).

We proceeded to use NOA for the rest of the studies as it was more anti-inflammatory than DHA and EPA and more cost-effective than NLA.

NOA-pDNA-LNPs show superior safety profiles in vitro and in vivo

To confirm that the reduction in IFN-β production of macrophages treated with NOA-pDNA-LNPs is due to STING inhibition, we performed confocal imaging for activated STING (p-STING). Four hours after 1,000 ng ml^{-1} dose, no measurable STING activation was observed in cells treated with NOA-pDNA-LNPs (Fig. 4a,b). We also did not detect activation of TANK-binding kinase 1 (TBK1), a downstream marker of STING activation, in cells that received NOA-pDNA-LNPs (Fig. 4c,d).

Furthermore, likely due to the reduced levels of pro-inflammatory cytokines, NOA-pDNA-LNPs maintained higher cell viability over time

compared with standard pDNA-LNPs, highlighting the protective effects of NOA in vitro (Fig. 4e). To generalize the anti-inflammatory effects of NOA, we loaded NOA into three different LNPs formulated with the same components found in the FDA-approved LNPs (D-Lin-MC3-DMA, SM-102 and ALC-0315). Regardless of the LNP composition, the addition of NOA led to a significant reduction in IFN-β secretion in cell supernatant 4 h after 1,000 ng ml^{-1} dose (Fig. 4f–h). Notably, the total levels of IFN-β varied with each ionizable lipid used (SM-102 > ALC-0315 > D-Lin-MC3-DMA), which we found also correlated with the transgene expression (Supplementary Fig. 11a–c). We found a similar trend in vivo with these ionizable lipids, especially when evaluating IFN-γ (Supplementary Fig. 11d).

Next, we investigated the safety profile of NOA-pDNA-LNPs in naive C57BL/6 mice. To assess the effect on acute response to pDNA, we i.v. injected 5 µg of standard pDNA-LNP or NOA-pDNA-LNP in mice and collected plasma 4 h later for cytokine quantification. We observed significantly lower levels of various pro-inflammatory cytokines (IFN-β, IL-1α, IFN-γ, TNF, MCP-1, IL-1β and IL-6) in mice treated with NOA-pDNA-LNPs compared with pDNA-LNPs (Fig. 4i). Specifically, IFN-β and IL-6 were reduced approximately four-fold and approximately eight-fold, respectively (Fig. 4j,k). By performing a dose–response study, we identified NOA-to-total lipid ratio (mole-to-mole) of 0.2–0.8 as the optimal formulation parameter in ameliorating pDNA-induced inflammation (Supplementary Fig. 12). We also observed that co-administration of NOA with pDNA-LNPs still had anti-inflammatory effects but to a lesser extent than when NOA was loaded into pDNA-LNPs (NOA-pDNA-LNPs) (Supplementary Fig. 13).

We attempted to further reduce the pDNA-induced inflammatory response by loading A151, an oligonucleotide previously shown to inhibit not only cGAS but also other DNA sensors, namely AIM2 and TLR9 (ref. 26). We observed some efficacy in vitro but did not see any additive or synergistic effects in vivo when co-loaded into NOA-pDNA-LNPs (Supplementary Fig. 14).

Notably, NOA-pDNA-LNPs completely prevented mortality in C57BL/6 mice compared with standard pDNA-LNPs at the 1 mg kg^{-1} dose (Fig. 4l). Further safety profile evaluation of pDNA-LNPs and NOA-pDNA-LNPs was done by performing histological examinations (hematoxylin and eosin (H&E)-stained liver, kidney and spleen) and other serum biomarkers such as alanine aminotransferase (ALT), aspartate aminotransferase (AST), creatinine (CREA) and blood urea nitrogen (BUN) levels. There was some disorientation of white pulp and brownish pigments in the red pulp area (black and white arrows, respectively) in the spleen for the pDNA-LNP and NOA-pDNA-LNP groups (Supplementary Fig. 15a). We also observed a small increase in AST and ALT, within a range seen with adeno-associated viruses (AAVs)[27]. No change was observed in BUN or CREA (Supplementary Fig. 15b–e). Thus, NOA did not eliminate all pDNA-associated inflammation, which is confirmed by the weight loss seen shown in Supplementary Fig. 16, but it is important to note that it has taken the mortality from 100% to 0% at the 1 mg kg^{-1} dose, which allows for further studies of pDNA-LNPs. Further studies will focus on engineering out residual inflammation before clinical translation of NOA-pDNA-LNPs.

NOA-pDNA-LNPs show prolonged transgene expression in vivo

We next investigated how the addition of NOA into pDNA-LNPs affects pDNA transgene expression. The duration of luciferase expression within the whole body of BALB/c mice was monitored after i.v. injection of 25 µg of either pDNA-LNPs or NOA-pDNA-LNPs using an in vivo imaging system (IVIS) (Fig. 5a). pDNA-LNP and NOA-pDNA-LNP showed similar levels of protein expression, confirming that the addition of NOA provides better safety profiles without hindering transgene expression in vivo (Fig. 5b). Notably, during this study, two mice that received 25 µg of pDNA-LNPs without NOA died within 2 d.

Furthermore, we i.v. injected 5 µg and 25 µg of mRNA-LNPs as controls and observed high but transient luciferase protein expression (Supplementary Fig. 17). It is also notable that luciferase transgene protein has an unusually long half-life for an intracellular protein, due to its lack of specific degradative pathways. Thus, luciferase requires long-term experiments to show the major difference in DNA versus mRNA expression kinetics. In addition, mice injected with NOA-pDNA-LNPs had significantly higher levels of luciferase protein even after 32 d compared with PBS and mRNA-LNP controls (Fig. 5c). Furthermore, we performed an ex vivo IVIS imaging study, which showed that pDNA-LNPs and NOA-pDNA-LNPs mainly express in liver and spleen (Supplementary Fig. 18). Lastly, we also showed that these NOA-pDNA-LNPs are redosable (Supplementary Fig. 19).

A small LNP formulation screen significantly boosts transgene expression of NOA-pDNA-LNPs in vitro

As a proof of concept, we investigated if we could improve protein expression from NOA-pDNA-LNPs. Typically, LNP formulation parameters, such as the type and amount of ionizable lipid and helper lipid, are optimized using a screening process to improve transgene expression. Unlike mRNA delivery, there are additional challenges for pDNA delivery, such as nuclear translocation, which is required for pDNA transcription and pDNA degradation due to endosomal and cytosolic DNases[28,29]. As such, many studies optimizing LNP formulation for mRNA delivery may not directly translate to improving pDNA delivery.

Thus, we first performed a small design of experiments (DoE) screen to find optimal formulation parameters for improving the transgene expression capacity of NOA-pDNA-LNPs. Using JMP software, we designed a full factorial DoE by varying three parameters: amount of ALC-0315 ionizable lipid (30–50 mole %), total lipid-to-pDNA ratio (10:1 to 40:1, w/w or N:P of 2.4–9.7) and the type of helper/charged lipid (DSPC, DOPE, DOTAP and 18:0 PG). All formulations contained NOA-to-total lipid ratio of 0.2 (mole-to-mole) and used a plasmid encoding luciferase protein. A total of 48 LNP formulations were tested in RAW264.7 cells at a dose of 500 ng ml^{-1} for 24 h before measuring luciferase protein expression. DoE results show how slight changes in the LNP formulation can affect pDNA transgene expression capacity (Fig. 6a). LNPs formulated with DSPC, DOPE or 18:0 PG as the helper/charged lipid had lower transgene expression compared with LNPs made with DOTAP (Supplementary Fig. 20). Notably, optimized LNPs with DOTAP as the helper lipid led to a 50-fold increase in pDNA transgene expression (Fig. 6b). Optimized NOA-pDNA-LNPs were made using 40% ALC-0315, 46.4% cholesterol, 12.1% DOTAP and 1.5% ALC-0519. We speculate that DOTAP can help condense and potentially protect pDNA from cytosolic degradation, leading to greater transgene expression, although further studies are required to elucidate the specific mechanisms.

To validate and generalize the optimized NOA-pDNA-LNP formulation to other cell types, we treated difficult-to-transfect cells, human iPSC-derived alveolar epithelial type II-like cells (iAT2s), and measured eGFP transgene expression over time. Representative images show improved transfection efficiencies of optimized NOA-pDNA-LNPs compared with the gold standard, Lipofectamine 2000 (Fig. 6c). Note that the tdTomato (red) signal indicates iAT2 cell positivity. One hundred twenty hours after treatment, iAT2s were collected, and flow cytometry was performed, which showed similar (but trending higher) percent eGFP positivity in cells treated with optimized NOA-pDNA-LNPs compared with the cells treated with Lipofectamine 2000 (Fig. 6d). Furthermore, optimized NOA-pDNA-LNPs also showed ability to transfect precision-cut lung slices (PCLSs) derived from human lungs (Supplementary Fig. 21).

Lastly, we observed that the in vitro results did not correlate to the in vivo results. We found that this was due to the fact that the addition of DOTAP altered the biodistribution of pDNA-LNPs, redirecting

some LNPs to the lungs and changing the overall expression capacity (Supplementary Fig. 22), a well-characterized phenomenon[30–32].

In conclusion, we demonstrate that the formulation of NOA-pDNA-LNPs can be iteratively optimized for specific applications, such as improving in vitro transfection in difficult-to-transfect cells as shown in this study, with further studies required for in vivo LNP optimization.

Discussion

Despite the success of nucleoside-modified mRNA-LNP therapeutics, the relatively short half-life of mRNA expression remains one of the biggest challenges limiting its application in the treatment of chronic diseases. In contrast, pDNA delivery should enable prolonged gene expression (months) and tunable promoters providing cell specificity and temporal control. However, here we show the acute toxicities associated with pDNA delivery via LNPs, triggering a high level of morbidity and even mortality at commonly used therapeutic doses in wild-type C57BL/6 and BALB/c mice.

Through immunofluorescence staining in vitro and genetic knockout mice in vivo, we identified STING activation as a primary driver of pDNA-LNP-induced adverse events. The acute response to pDNA-LNPs is highlighted by the rapid onset of lethargy and lack of movement in mice within hours after LNP administration, culminating in 100% mortality within 2 d at the 1 mg kg^{-1} dose. Furthermore, we show that this acute-but-transient inflammatory response occurs across various pDNA-LNP formulations with varying lipid and pDNA components.

To increase the safety profile of pDNA-LNPs, we introduce a technology in which endogenous anti-inflammatory lipids with STING inhibitory activity are loaded into standard pDNA-LNP formulations. We show that various AILs can be loaded into standard pDNA-LNPs without negatively affecting pDNA loading or particle stability. Specifically, we demonstrate the efficacy of NOA in mitigating pDNA-induced inflammation both in vitro and in vivo. By incorporating NOA into pDNA-LNPs, we achieved a significant reduction in pro-inflammatory cytokine levels and adverse events, without compromising transgene expression efficiency.

Moreover, NOA-pDNA-LNPs express the transgene for at least 1 month compared with approximately 2 weeks for mRNA-LNPs. We also show that the NOA-pDNA-LNP formulation can be optimized for improving expression by performing a DoE screen, revealing critical LNP formulation parameters on pDNA expression capacity. Optimized NOA-pDNA-LNPs with DOTAP as the helper lipid exhibit superior transfection efficiency compared with standard NOA-pDNA-LNPs (50-fold increase) in RAW264.7 cells and similar efficiencies to the gold standard, Lipofectamine, even in human iPSC-derived type II alveolar epithelial cells (iAT2s) that are known to be difficult to transfect. Mechanistically, this increase in expression warrants further investigation, although we speculate that it is likely due to improved protection and/or condensation of pDNA.

The incorporation of bioactive molecules, such as NOA, into pDNA-LNPs represents an initial step toward addressing the challenges associated with pDNA-LNP delivery. Further studies are needed to address the inefficiencies in DNA-LNP transfection, which we hypothesize stem from intracellular pDNA degradation and limited nuclear translocation. Although NOA-pDNA-LNPs significantly mitigated systemic inflammation, their efficacy in specific tissue contexts requires further validation. Beyond LNP engineering, as demonstrated in this study, advancements in DNA engineering to explore and evaluate various structural designs could provide deeper insights into the mechanisms underlying DNA-LNP-induced STING activation.

In conclusion, our study highlights the need to address the adverse events associated with pDNA-LNP administration and presents an approach to enhance the safety and efficacy of non-viral pDNA delivery. Loading pDNA-LNPs with bioactive molecules, such as NOA, will add pDNA-LNPs to the genetic medicine toolbox alongside the other clinically validated tools of mRNA-LNPs, siRNA, CRISPR and AAVs.

Online content

Any methods, additional references, Nature Portfolio reporting summaries, source data, extended data, supplementary information, acknowledgements, peer review information; details of author contributions and competing interests; and statements of data and code availability are available at https://doi.org/10.1038/s41587-025-02556-5.

References

1. Tenchov, R., Bird, R., Curtze, A. E. & Zhou, Q. Lipid nanoparticles—from liposomes to mRNA vaccine delivery, a landscape of research diversity and advancement. *ACS Nano* **15**, 16982–17015 (2021).
2. Hou, X., Zaks, T., Langer, R. & Dong, Y. Lipid nanoparticles for mRNA delivery. *Nat. Rev. Mater.* **6**, 1078–1094 (2021).
3. Pardi, N. et al. Expression kinetics of nucleoside-modified mRNA delivered in lipid nanoparticles to mice by various routes. *J. Control. Release* **217**, 345–351 (2015).
4. Herweijer, H. et al. Time course of gene expression after plasmid DNA gene transfer to the liver. *J. Gene Med.* **3**, 280–291 (2001).
5. Das, A. T., Tenenbaum, L. & Berkhout, B. Tet-On systems for doxycycline-inducible gene expression. *Curr. Gene Ther.* **16**, 156–167 (2016).
6. Arjomandnejad, M., Dasgupta, I., Flotte, T. R. & Keeler, A. M. Immunogenicity of recombinant adeno-associated virus (AAV) vectors for gene transfer. *BioDrugs* **37**, 311–329 (2023).
7. Bulcha, J. T., Wang, Y., Ma, H., Tai, P. W. L. & Gao, G. Viral vector platforms within the gene therapy landscape. *Signal Transduct. Target. Ther.* **6**, 53 (2021).
8. Zhu, Y. et al. Multi-step screening of DNA/lipid nanoparticles and co-delivery with siRNA to enhance and prolong gene expression. *Nat. Commun.* **13**, 4282 (2022).
9. Guimaraes, L. C. et al. Nanoparticle-based DNA vaccine protects against SARS-CoV-2 variants in female preclinical models. *Nat. Commun.* **15**, 590 (2024).
10. Liao, H.-C. et al. Lipid nanoparticle-encapsulated DNA vaccine robustly induce superior immune responses to the mRNA vaccine in Syrian hamsters. *Mol. Ther. Methods Clin. Dev.* **32**, 101169 (2024).
11. Nguyen, T. N. et al. Lipid nanoparticle-encapsulated DNA vaccine confers protection against swine and human-origin H1N1 influenza viruses. *mSphere* **9**, e0028324 (2024).
12. Yu, L. & Liu, P. Cytosolic DNA sensing by cGAS: regulation, function, and human diseases. *Signal Transduct. Target. Ther.* **6**, 170 (2021).
13. Cheng, Z. et al. The interactions between cGAS-STING pathway and pathogens. *Signal Transduct. Target. Ther.* **5**, 91 (2020).
14. Hansen, A. L. et al. Nitro-fatty acids are formed in response to virus infection and are potent inhibitors of STING palmitoylation and signaling. *Proc. Natl Acad. Sci. USA* **115**, E7768–E7775 (2018).
15. Pardi, N. et al. Administration of nucleoside-modified mRNA encoding broadly neutralizing antibody protects humanized mice from HIV-1 challenge. *Nat. Commun.* **8**, 14630 (2017).
16. Chase, L. S., Zaleski, M. H., Morrell, L. J. & Brenner, J. S. Automated measurement of distance-walked as a 'sixth vital sign' for detecting infusion reactions during preclinical testing. *Int. J. Pharm.* **645**, 123369 (2023).
17. Domizio, J. D. et al. The cGAS–STING pathway drives type I IFN immunopathology in COVID-19. *Nature* **603**, 145–151 (2022).
18. Zhang, X., Goel, V. & Robbie, G. J. Pharmacokinetics of patisiran, the first approved RNA interference therapy in patients with hereditary transthyretin-mediated amyloidosis. *J. Clin. Pharmacol.* **60**, 573–585 (2020).

19. Schoenmaker, L. et al. mRNA-lipid nanoparticle COVID-19 vaccines: structure and stability. *Int. J. Pharm.* **601**, 120586 (2021).
20. Parhiz, H. et al. Added to pre-existing inflammation, mRNA-lipid nanoparticles induce inflammation exacerbation (IE). *J. Control. Release* **344**, 50–61 (2022).
21. Banete, A., Barilo, J., Whittaker, R. & Basta, S. The activated macrophage—a tough fortress for virus invasion: how viruses strike back. *Front. Microbiol.* **12**, 803427 (2022).
22. Sasaki, A. & Kinjo, M. Monitoring intracellular degradation of exogenous DNA using diffusion properties. *J. Control. Release* **143**, 104–111 (2010).
23. Wang, D., Zhao, H., Shen, Y. & Chen, Q. A variety of nucleic acid species are sensed by cGAS, implications for its diverse functions. *Front. Immunol.* **13**, 826880 (2022).
24. Melo, T., Montero-Bullón, J.-F., Domingues, P. & Domingues, M. R. Discovery of bioactive nitrated lipids and nitro-lipid-protein adducts using mass spectrometry-based approaches. *Redox Biol.* **23**, 101106 (2019).
25. Khoo, N. K. H., Li, L., Salvatore, S. R., Schopfer, F. J. & Freeman, B. A. Electrophilic fatty acid nitroalkenes regulate Nrf2 and NF-κB signaling: a medicinal chemistry investigation of structure-function relationships. *Sci. Rep.* **8**, 2295 (2018).
26. Kaminski, J. J. et al. Synthetic oligodeoxynucleotides (ODN) containing suppressive TTAGGG motifs inhibit AIM2 inflammasome activation. *J. Immunol.* **191**, 3876–3883 (2013).
27. Tao, R. et al. Long-term metabolic correction of phenylketonuria by AAV-delivered phenylalanine amino lyase. *Mol. Ther. Methods Clin. Dev.* **19**, 507–517 (2020).
28. Sperinde, J. J., Choi, S. J. & Szoka, F. C. Phage display selection of a peptide DNase II inhibitor that enhances gene delivery. *J. Gene Med.* **3**, 101–108 (2001).
29. Bai, H., Lester, G. M. S., Petishnok, L. C. & Dean, D. A. Cytoplasmic transport and nuclear import of plasmid DNA. *Biosci. Rep.* **37**, BSR20160616 (2017).
30. Cheng, Q. et al. Selective organ targeting (SORT) nanoparticles for tissue-specific mRNA delivery and CRISPR–Cas gene editing. *Nat. Nanotechnol.* **15**, 313–320 (2020).
31. Wei, T. et al. Lung SORT LNPs enable precise homology-directed repair mediated CRISPR/Cas genome correction in cystic fibrosis models. *Nat. Commun.* **14**, 7322 (2023).
32. Omo-Lamai, S. et al. Physicochemical targeting of lipid nanoparticles to the lungs induces clotting: mechanisms and solutions. *Adv. Mater.* **36**, e2312026 (2024).

Methods

Materials

Ionizable lipids (D-Lin-MC3-DMA, ALC-0315 and SM-102), ALC-0159 and NOA were purchased from Echelon Biosciences (catalog numbers N-1282, N-1102, N-1020, N-2010 and L-0112, respectively). DHA was purchased from MedChemExpress (catalog number HY-B2167). EPA and NLA were purchased from Cayman Chemical (catalog numbers 90110 and 30160, respectively). 18:0 PC (DSPC, 1,2-distearoyl-sn-glycero-3-phosphocholine), DMG-PEG 2000 (1,2-dimyristoyl-rac-glycero-3-methoxypolyethylene glycol-2000), 18:0 TAP (DOTAP, 1,2-stearoyl-3-trimethylammonium-propane (chloride salt)), 18:1 (Δ9-cis) PE (DOPE, 1,2-dioleoyl-sn-glycero-3-phosphoethanolamine) and 18:0 PG (1,2-distearoyl-sn-glycero-3-phospho-(1′-rac-glycerol) (sodium salt)) were purchased from Avanti Polar Lipids (catalog numbers 850365, 880151, 890880, 850725 and 840465, respectively). Plasmid DNA was purchased from Aldevron (<0.1 EU μl^{-1} endotoxin level, catalog number 5078-5). 5moU nucleoside-modified firefly luciferase mRNA was purchased from TriLink BioTechnologies (catalog number L-7202).

Animals

All animal experiments strictly adhered to the guidelines established in the Guide for the Care and Use of Laboratory Animals (National Institutes of Health). Approval for all animal procedures was obtained from the University of Pennsylvania Institutional Animal Care and Use Committee. Naive C57BL/6, naive BALB/c, STING-KO BALB/c and C57BL/6 mice, AIM2-knockout C57BL/6 mice and TLR9-knockout C57BL/6 mice, aged 6–8 weeks and weighing 23–25 g, were procured from The Jackson Laboratory for the study. The mice were housed in a controlled environment, maintained at temperatures between 22 °C and 26 °C with a 12-h light/dark cycle, and provided with access to food and water.

LNP formulation

LNPs were formulated using microfluidics (Precision NanoSystems, NanoAssemblr Ignite). Lipids were dissolved in ethanol and mixed with aqueous buffer (50 mM citrate buffer, pH 4) containing either 5moU nucleoside-modified mRNA or pDNA, at a total flow rate of 6 ml min^{-1}, a flow rate ratio of 1-to-3 (ethanol-to-aqueous) and a total lipid-to-nucleic acid ratio of 40-to-1 (w/w; that is, N:P ratio of 9.7). LNPs were dialyzed against 1× PBS in a 12–14 kDa molecular weight cutoff cassette for 2 h, stored at 4 °C and used within 2 d. AILs were added as a fifth component at an AIL-to-total lipid ratio of 0.2 (mole-to-mole) for all studies using AIL-loaded pDNA-LNPs unless otherwise indicated.

All LNPs were made using the FDA-approved formulation parameters with the following molar ratios: D-Lin-MC3-DMA LNPs: 50% D-Lin-MC3-DMA, 38.5% cholesterol, 10% DSPC and 1.5% DMG-PEG 2000; SM-102 LNPs: 50% SM-102, 38.5% cholesterol, 10% DSPC and 1.5% DMG-PEG 2000; and ALC-0315 LNPs: 46.3% ALC-0315, 42.7% cholesterol, 9.4% DSPC and 1.6% ALC-0159. All studies used the ALC-0315 LNP formulation unless otherwise indicated.

LNP characterization

Measurements of hydrodynamic nanoparticle size and polydispersity index were conducted through DLS using a Zetasizer Pro ZS (Malvern Panalytical). The encapsulation efficiencies and concentrations of LNP mRNA or pDNA were determined using a Quant-iT RiboGreen RNA assay or a Quant-iT PicoGreen dsDNA assay, respectively (Invitrogen). AIL loading in LNP was determined using UPLC (UV/Vis) after purifying out unloaded AILs using size exclusion Zeba spin desalting columns (Thermo Fisher Scientific, catalog number 89877) as previously described[33]. In brief, a Waters Acquity I-Class UPLC system was used, consisting of a Binary Solvent Manager, Sample Manager-FTN and photo diode array (PDA) detector. Chromatography was performed using a gradient method and a Cortecs C18 column (1.6-µm particle size, 2.1 × 50 mm). Mobile phase A was water with 0.1 vol% trifluoroacetic acid (TFA); mobile phase B was acetonitrile with 0.1 vol% TFA. The flow rate was 0.5 ml min^{-1} with a gradient of 10% B from 0 min to 0.4 min, linearly increasing to 90% B from 0.4 min to 0.8 min, holding at 90% B from 0.8 min to 1.3 min and then linearly decreasing to 10% B from 1.3 min to 1.4 min. The sample injection volume was 8 µl, and the retention time for NOA was approximately 1.5 min. UPLC analysis was done using Empower (version 3) software.

Cell culture

RAW264.7 mouse macrophages were purchased from the American Type Culture Collection and cultured in DMEM with 10% heat-inactivated FBS and 1% penicillin–streptomycin. All cells were incubated with 5% CO_2 at 37 °C.

For cell viability and luciferase assays, cells were seeded at a density of 1×10^5 cells per well in a 96-well (clear bottom for cell viability assay and white bottom for luciferase assay) plate using 100 µl 24 h before LNP treatment. A cck8 assay (catalog number ab228554) was performed according to the manufacturer's instructions to measure cell viability percent (Abcam; absorbance was measured using a SpectraMax M2 plate reader, version 5.4). The 'Luciferase Assay Systems' protocol was used to measure expression capacity of either mRNA or pDNA LNPs in vitro (Promega).

For cytokine studies, cells were seeded at a density of 3×10^5 cells per well in a 24-well clear-bottom plate using 300 µl 24 h before LNP treatment. Four hours after LNP treatment, the supernatant was collected, spun down at 10,000*g* for 10 min to remove any debris and stored at −80 °C.

For immunofluorescence imaging studies, cells were seeded at a density of 1.2×10^5 cells per well in eight-well µ-Slide chambers.

p-STING and p-TBK1 imaging and quantification

Cells were treated with LNPs for 4 h. Then, they were fixed in 4% fresh paraformaldehyde for 15 min. Permeability was then performed with 0.05% saponin buffer (Invitrogen, J63209.AK) for 10 min. Next, samples were incubated with 10% normal goat serum (Life Technologies, 50062Z) for 1 h. After PBS washing, cells were treated with 1:150 primary antibodies (Cell Signaling Texchnology, anti p-STING, 62912S; Cell Signaling Technology, anti p-TBK1, 5483S) at 4 °C overnight. Cells were washed with PBS to remove unbound antibodies. Then, cells were incubated with 1:750 secondary antibodies (Invitrogen; Alexa Fluor 488–conjugated goat anti-rabbit antibody, A11008) at 37 °C for 1.5 h. Cell nuclei were labeled using DAPI. Images were acquired by LSM 980 microscopy (Zeiss), and mean fluorescence intensity (MFI) was measured by ImageJ (1.53k).

iPSC-derived alveolar type 2 epithelial cell transfection

Alveolar type 2 epithelial cells derived from human iPSCs (iAT2s) were maintained in 3D growth factor reduced (GFR)-Matrigel culture as previously described[34,35]. Plating iAT2s on 2D transwell inserts (Falcon; 6.5 mm) was performed as previously described[36]. In brief, transwell inserts were coated with diluted hESC-Qualified Matrigel (Corning) as instructed by the manufacturer. A single-cell suspension of iAT2s from 3D culture was obtained by dissociating Matrigel droplets for 30 min with 2 mg ml^{-1} Dispase (Gibco) followed by 15 min of 0.05% trypsin-EDTA (Gibco) at 37 °C. iAT2s were plated on pre-coated transwell inserts at a density of 500,000 live cells per cm^2 in 500 µl of CK + DCI + Y (3 µM CHIR99021, 10 ng ml^{-1} KGF, 50 nM dexamethasone, 0.1 mM cAMP, 0.1 mM IBMX, 10 µM Rho-associated kinase inhibitor (Y) (MilliporeSigma, Y-27632)), with 500 µl of CK + DCI + Y added to the basolateral compartment. Forty-eight hours after plating, iAT2s were refreshed with 500 µl of CK + DCI in both the apical and basolateral compartments before LNP administration and transfection.

Various conditions of LNPs containing eGFP pDNA were administered dropwise onto 2D cultures of iAT2s. Lipofectamine 2000 (Thermo Fisher Scientific) transfection of eGFP pDNA was performed according to the manufacturer's protocol. iAT2s were imaged for tdTomato retention and eGFP expression using an Eclipse Ti2 Series inverted microscope (Nikon) and 24 h, 48 h and 120 h after treatment. After 120 h,

iAT2s were isolated from transwell inserts with Accutase (STEMCELL Technologies) and washed in FACS buffer (0.1% BSA, 2 mM EDTA, in PBS pH 7.4) for flow cytometry analysis. iAT2 tdTomato retention and eGFP expression were assessed by flow cytometry using a CytoFLEX SRT (Beckman Coulter) and analyzed using FlowJo version 10.10 software.

Transfection of PCLSs from human lung tissues

Human PCLSs of 300 µm were cultured in DMEM with 10% FBS and 1% Primocin overnight at 37 °C. eGFP pDNA (1,000 ng ml^{-1}) and Lipofectamine 2000 (catalog number 11668) were mixed in Opti-MEM before adding to PCLSs. Optimized NOA-pDNA-LNPs (1,000 ng ml^{-1}) were prepared in DMEM with 10% FBS and 1% Primocin. Treatments were added in PCLSs cultured in DMEM with 10% FBS and 1% Primocin and incubated overnight at 37 °C. Twenty-four hours after treatment, eGFP tissue imaging was performed using a Leica confocal microscope. The aspect ratio of the images was reduced 3:5 followed by 4:5 two times to highlight the area of interest.

In vivo studies

For survival curve studies, mice were monitored and weighed daily. Any mice with visual cues of extreme distress or weight loss more than 20% were euthanized and removed from the study. All i.v. injections were done retro-orbitally by injecting into the retro-bulbar sinus.

For plasma collection, mice treated with LNPs were euthanized by terminal blood collection via inferior vena cava. Opening of the major body cavity and subsequent thoracotomy was performed as a secondary measure of euthanization. Blood was centrifuged at 1,000*g* for 10 min (room temperature), and then plasma supernatant was collected and stored at −80 °C.

*C*ytokine measurements were carried out on plasma (2× diluted) or cell culture supernatant (undiluted) with a LEGENDplex 13-plex Mouse Inflammation Panel (BioLegend, catalog number 740150) according to the manufacturer's instructions.

For in vivo imaging studies, mice were intraperitoneally injected with 100 µl of 30 mg ml^{-1} D-luciferin sodium salt (Regis Technologies, 103404-75-7) under 3% isoflurane-induced anesthesia and then placed in an IVIS Spectrum machine (PerkinElmer) belly up and imaged for whole-body chemiluminescence every 0.2 min with automatically determined exposure time for 10–12 images, until the signal reached the peak intensity. PerkinElmer Living Image software (version 4.5.5) was used to analyze images.

Statistics

All results are expressed as mean ± s.e.m. unless specified otherwise. Statistical analyses were performed using GraphPad Prism 8 (GraphPad Software). * denotes $P < 0.05$, ** denotes $P < 0.01$, *** denotes $P < 0.001$ and **** denotes $P < 0.0001$.

Reporting summary

Further information on research design is available in the Nature Portfolio Reporting Summary linked to this article.

Data availability

All quantitative data used for plots in figures are available in the Source data file. mRNA and pDNA sequences are in Supplementary Tables 1 and 2. Source data are provided with this paper.

References

33. Zaleski, M. H. et al. Nanocarriers' repartitioning of drugs between blood subcompartments as a mechanism of improving pharmacokinetics, safety, and efficacy. *J. Control. Release* **374**, 425–440 (2024).
34. Jacob, A. et al. Differentiation of human pluripotent stem cells into functional lung alveolar epithelial cells. *Cell Stem Cell* **21**, 472–488 (2017).
35. Jacob, A. et al. Derivation of self-renewing lung alveolar epithelial type II cells from human pluripotent stem cells. *Nat. Protoc.* **14**, 3303–3332 (2019).
36. Abo, K. M. et al. Air–liquid interface culture promotes maturation and allows environmental exposure of pluripotent stem cell–derived alveolar epithelium. *JCI Insight* **7**, e155589 (2022).

Acknowledgements

Research reported in this publication was supported by the American Heart Association under grant 24PRE1195406 (to M.N.P.), grants R01-HL-153510, R01-HL160694 and R01-HL164594 (to J.S.B.) and grant R01AI153064 (to N.P.). We thank the laboratories of D. Kotton and K.-D. Alysandroatos for gifting alveolar type 2 epithelial cells derived from human induced pluripotent stem cells (iAT2s). Figures 1b, 2a and 3a,b were created with BioRender.com.

Author contributions

M.N.P. and S.T.: project administration, methodology, investigation, formal analysis, data curation, conceptualization, writing—review and editing, and writing—original draft. Y.W. and S.O.: methodology, investigation, formal analysis, data curation and writing—review and editing. J.W., S.O.-L., C.E., L.S.C., A.M., E.H. and A. Shah: methodology, investigation and data curation. A. Sárközy: methodology. J.K.: resources, methodology and supervision. N.P.: resources, funding acquisition, writing—review and editing, and supervision. J.S.B.: visualization, resources, methodology, funding acquisition, formal analysis, data curation, conceptualization, writing—review and editing, and supervision.

Competing interests

M.N.P., S.T. and J.S.B. have filed a patent for the DNA-LNP technology described herein. The other authors declare no competing interests.

Additional information

Supplementary information The online version contains supplementary material available at https://doi.org/10.1038/s41587-025-02556-5.

Correspondence and requests for materials should be addressed to Jacob S. Brenner.

Peer review information *Nature Biotechnology* thanks Anna Blakney and the other, anonymous, reviewer(s) for their contribution to the peer review of this work.

nature portfolio

Corresponding author(s): Jacob S. Brenner

Last updated by author(s): 01/04/2025

Reporting Summary

Nature Portfolio wishes to improve the reproducibility of the work that we publish. This form provides structure for consistency and transparency in reporting. For further information on Nature Portfolio policies, see our Editorial Policies and the Editorial Policy Checklist.

Statistics

For all statistical analyses, confirm that the following items are present in the figure legend, table legend, main text, or Methods section.

n/a	Confirmed
☐	☒ The exact sample size (*n*) for each experimental group/condition, given as a discrete number and unit of measurement
☐	☒ A statement on whether measurements were taken from distinct samples or whether the same sample was measured repeatedly
☐	☒ The statistical test(s) used AND whether they are one- or two-sided *Only common tests should be described solely by name; describe more complex techniques in the Methods section.*
☒	☐ A description of all covariates tested
☐	☒ A description of any assumptions or corrections, such as tests of normality and adjustment for multiple comparisons
☐	☒ A full description of the statistical parameters including central tendency (e.g. means) or other basic estimates (e.g. regression coefficient) AND variation (e.g. standard deviation) or associated estimates of uncertainty (e.g. confidence intervals)
☐	☒ For null hypothesis testing, the test statistic (e.g. *F*, *t*, *r*) with confidence intervals, effect sizes, degrees of freedom and *P* value noted *Give P values as exact values whenever suitable.*
☒	☐ For Bayesian analysis, information on the choice of priors and Markov chain Monte Carlo settings
☒	☐ For hierarchical and complex designs, identification of the appropriate level for tests and full reporting of outcomes
☒	☐ Estimates of effect sizes (e.g. Cohen's *d*, Pearson's *r*), indicating how they were calculated

Our web collection on statistics for biologists contains articles on many of the points above.

Software and code

Policy information about availability of computer code

Data collection	UPLC: Waters, Acquity (cortecs column C18 1.6 µm) Absorbance and Fluorescence intensity: Molecular Devices, SpectraMax M2 IVIS: PerkinElmer Flow Cytometry: Beckman CytoFlex SRT Luminescence: Promega
Data analysis	UPLC: Empower (V3) Absorbance and Fluorescence intensity: SoftMax Pro (V5.4) IVIS: PerkinElmer Living Image Software (V4.5.5) Imaging: ImageJ 1.53k

For manuscripts utilizing custom algorithms or software that are central to the research but not yet described in published literature, software must be made available to editors and reviewers. We strongly encourage code deposition in a community repository (e.g. GitHub). See the Nature Portfolio guidelines for submitting code & software for further information.

Data

Policy information about availability of data

All manuscripts must include a data availability statement. This statement should provide the following information, where applicable:

- Accession codes, unique identifiers, or web links for publicly available datasets
- A description of any restrictions on data availability
- For clinical datasets or third party data, please ensure that the statement adheres to our policy

All quantitative data used for plots in figures is available in the Source Data file. Additional data is available upon reasonable request from the corresponding author.

Research involving human participants, their data, or biological material

Policy information about studies with human participants or human data. See also policy information about sex, gender (identity/presentation), and sexual orientation and race, ethnicity and racism.

Reporting on sex and gender	N/A
Reporting on race, ethnicity, or other socially relevant groupings	N/A
Population characteristics	N/A
Recruitment	N/A
Ethics oversight	N/A

Note that full information on the approval of the study protocol must also be provided in the manuscript.

Field-specific reporting

Please select the one below that is the best fit for your research. If you are not sure, read the appropriate sections before making your selection.

☒ Life sciences ☐ Behavioural & social sciences ☐ Ecological, evolutionary & environmental sciences

For a reference copy of the document with all sections, see nature.com/documents/nr-reporting-summary-flat.pdf

Life sciences study design

All studies must disclose on these points even when the disclosure is negative.

Sample size	Sample sizes were determined based on our statistical threshold (alpha = 0.05, power >= 80%) and historical sample sizes used.
Data exclusions	No data was excluded from analysis.
Replication	Key in vivo studies such as Figure 1a,1d , Figure 4i-l, and Figure 5b were replicated 3 times with similar results.
Randomization	To minimize variance, in vivo studies utilized similarly aged mice (6-8 weeks). Experimental groups were randomized by distributing across multiple cages. Other study materials (such as wells for in vitro testing) were all put randomly into different groups.
Blinding	Blinding was not logistically feasible during data analysis as one of the lead authors (M.N.P.) conducted all of the in vivo experiments, S.J.O. conducted all of the non-imaging in vitro experiments, and Y.W. performed the imaging in vitro experiments.

Reporting for specific materials, systems and methods

We require information from authors about some types of materials, experimental systems and methods used in many studies. Here, indicate whether each material, system or method listed is relevant to your study. If you are not sure if a list item applies to your research, read the appropriate section before selecting a response.

Materials & experimental systems

n/a	Involved in the study
☒	☐ Antibodies
☒	☐ Eukaryotic cell lines
☒	☐ Palaeontology and archaeology
☒	☐ Animals and other organisms
☒	☐ Clinical data
☒	☐ Dual use research of concern
☒	☐ Plants

Methods

n/a	Involved in the study
☒	☐ ChIP-seq
☒	☐ Flow cytometry
☒	☐ MRI-based neuroimaging

Plants

Seed stocks

Report on the source of all seed stocks or other plant material used. If applicable, state the seed stock centre and catalogue number. If plant specimens were collected from the field, describe the collection location, date and sampling procedures.

Novel plant genotypes

Describe the methods by which all novel plant genotypes were produced. This includes those generated by transgenic approaches, gene editing, chemical/radiation-based mutagenesis and hybridization. For transgenic lines, describe the transformation method, the number of independent lines analyzed and the generation upon which experiments were performed. For gene-edited lines, describe the editor used, the endogenous sequence targeted for editing, the targeting guide RNA sequence (if applicable) and how the editor was applied.

Authentication

Describe any authentication procedures for each seed stock used or novel genotype generated. Describe any experiments used to assess the effect of a mutation and, where applicable, how potential secondary effects (e.g. second site T-DNA insertions, mosiacism, off-target gene editing) were examined.